Contribution of the capillary pressure second-order term on fast drying of cement-based materials

Yuliang Zou, Mazen Saad, Frédéric Grondin

Version of Record: https://www.sciencedirect.com/science/article/pii/S095006182101182X
Manuscript_f30d0983da2f75df05ab7bed9f5d71f5

Contribution of the capillary pressure second-order term on fast drying of cement-based materials

Yuliang Zou[a,b], Mazen Saad[a], Frédéric Grondin[b,*]

[a] *Laboratoire de Mathématiques Jean Leray (LMJL), CNRS UMR 6629, Centrale Nantes, 1 rue de la Noë 44321 Nantes, France*
[b] *Institut de Recherche en Génie Civil et Mécanique (GeM), UMR 6183, Centrale de Nantes - Université de Nantes - CNRS, 1 rue de la Noë, 44321 Nantes, France*

Abstract

Standard models used to predict moisture transport of cement-based materials are based on quasi-static behaviour laws. However, it is not appropriate for fast drying condition. In this paper, a model taking into account dynamic effects on capillarity pressure is presented for the analysis of moisture transport in deforming cement-based materials. The proposed model is discretized in space by finite element method and in time by an implicit approximation-backward Euler method. On the basis of a drying experiment for cement paste, the dynamic model and non-dynamic model have been implemented and compared. Experimental data verifications indicate that dynamic model gives better results than static one. Moreover, the comparisons of numerical simulations reveal that dynamic capillarity effect has non-negligible influence on deformation and permeability. All investigations allow concluding that dynamic effects on capillary pressure should be taken into account to quantify moisture transport for fast drying condition.

Keywords: Cement paste, Fast drying, Finite Element Modelling, Dynamic pressure, Fluid-solid coupling

*Corresponding author. Tel.: +33 (0) 2 40 37 16 68
Email addresses: yuliang.zou@ec-nantes.fr (Yuliang Zou), mazen.saad@ec-nantes.fr (Mazen Saad), frederic.grondin@ec-nantes.fr (Frédéric Grondin)

1. Introduction

This study aims to explore why drying of concrete has different kinetics under different environmental relative humidity (RH) conditions. It is expected that the climate variation results in wetting-drying cycles in concrete structures. These cycles are the main cause of great swelling and shrinkage phenomena. Many experimental studies have shown that when deformations induced by these phenomena exceed a strength threshold, cracks are formed in the cement matrix and decrease the durability of concrete [1]. Essentially, the moisture state determines the distribution of capillary pressure which is the driving force for shrinkage and swelling of concrete. Therefore, these moisture transport and deformation must be mastered.

Predictive models have been developed to calculate the influence of wetting-drying cycles on deformation of concrete. Most of them are based on simple quasi-static fluid flow. Occasionally, the deformation variation is taken into account to modify the porosity and the permeability coefficient during the drying evolution. However, these models can only simulate drying for high external relative humidities for which the drying kinetic is slow and can be simulated by a quasi-static model. In case of low external relative humidity, some authors calibrate the exchange coefficient between the material and the environment according to the moisture kinetic [2]. Others consider higher permeability coefficients in order to increase the mass loss as measured in experiment [3]. Authors have explained this observation by assuming that more cracks appear during shrinkage. Previously, Day et al. [4] has suggested this assumption, but also indicated that it could be due to capillary tension forces. In our opinion, in a first approximation it is more relevant to develop a descriptive model to understand the role of each phenomenon in the global behaviour. So, how to consider physics effects in modelling to analyze the fast drying under low external relative humidity conditions?

The pressure difference between gas mixture and liquid water could deviate from the original static capillary pressure under dynamic situation in which viscous forces are non-negligible and need unexpected pressure gradient to overcome [5]. The term "dynamic" used in this paper is in the sense of the fluids mechanics. It means that the potential influence caused by fluid velocity is taken into account in the pore. The capillary pressure-saturation ($P_c - S_w$) relationship is crucial

to predict multi-phase flow in porous media [6]. It was detected that $P_c - S_w$ relation, determined under dynamic condition that the pressure equilibrium has not been established, deviates from the static equilibrium $P_c - S_w$ relation [7–9]. It can be explained by a theory of dynamic effects on capillary pressure [10]. Dynamic effects are dependent on time rate of change of saturation and permeability of porous media [11, 12]. So, the term dynamic is used here in the sense of the fluid mechanic while the fluid velocity is considered. Dynamic is not considered for the solid matter which has a static behaviour. Considerable quantitative relations have been introduced to characterize the influence of dynamic saturation variation on capillary pressure [5, 10, 13–16]. Among them, the work proposed by Hassanizadeh et al. [15] is well-known and widely used.

In recent decades, Considerable attention has been paid to unsaturated flow in quite permeable materials with dynamic effects considered [10, 17–19]. However, these well-developed dynamic capillarity effect theories have not been applied to weakly permeable materials (cement-based materials). Compared with quite permeable materials, the moisture transport in weakly permeable materials, which consists of Darciean water flow and Fickean vapour diffusion, is more complicated. Moreover, by-also known moisture transport determines evolution of capillary pressure, which is the main cause of the delayed deformations and occurrence of micro-cracks in cement-based materials [1, 20]. Thus, the consideration of dynamic effects on coupling of moisture transport and shrinkage is a challenging and urgent task.

This paper aims to present an advanced model with consideration of dynamic capillarity effect and skeleton deformation for fast drying of cement-based materials. In this paper, this model will be called "coupled dynamic model" while when the deformation skeleton is not taken into account it will be called "uncoupled dynamic model"; and "standard model" will be used when the dynamic capillarity effect is not taken into account. First, the derivation of this coupled dynamic model is introduced in detail. Then drying experiments of a kind of cement paste have been employed for the verification of this advanced model. Modeling results based on dynamic effects and non-dynamic effects are compared with experimental one. The last part investigates the skeleton deformation performed with dynamic effects and no-dynamic effects modeling.

2. Governing model for moisture transport in deforming porous media

2.1. Moisture transport from standard to dynamic model

Plenty of research results have proved that unsaturated moisture transport in weakly permeable porous media like cementitious material is composed of advective transport of liquid water and the advection-diffusion of gas mixture consisting of water vapour and dry air [21, 22]. The typical mass conservation equation for moisture transfer in porous material is written as follows:

$$\frac{\partial\left(\phi S_w \rho_w\right)}{\partial t}+\frac{\partial\left[\phi(1-S_w)\rho_v\right]}{\partial t}+\frac{\partial\left[\phi(1-S_w)\rho_a\right]}{\partial t}+\nabla\cdot\left(\rho_w V_w+\rho_v V_v+\rho_a V_a\right)=0 \tag{1}$$

where subscripts w, v, a represent respectively liquid water, vapour and dry air, ρ the density, V the velocity, ϕ the effective porosity, S_w the saturation of liquid water. For a deformable porous medium, the effective porosity can be expressed as follows:

$$\phi=\frac{\phi_0+\varepsilon_v}{1+\varepsilon_v} \tag{2}$$

where ϕ_0 represents the initial intrinsic porosity and ε_v the volumetric strain.

Considering the gaseous phases have much lower densities compared with liquid water, the second and third terms at the left-hand side of the equation (1) is considered negligible. An earlier study has justified that dry air transport has very weak contribution to total mass transport and only causes fluctuated air pressure in the material [23]. Similar conclusion was also obtained by the asymptotic analysis implemented by Coussy [22]. Besides, because of the liquid water is assumed incompressible, the initial mass conservation (equation 1) can be simplified by the following equation regarding liquid water and water vapour [21, 24]:

$$\rho_w\frac{\partial\left(\phi S_w\right)}{\partial t}+\nabla\cdot\left(\rho_w V_w+\rho_v V_v\right)=0. \tag{3}$$

The advective velocity of water V_w is defined by Extend Darcy's law:

$$V_w=-\frac{k k_{rw}}{\eta_w}\nabla P_w \tag{4}$$

where k, k_{rw}, η_w, P_w represent effective permeability, relative permeability, water viscosity, water pressure respectively. Taking into account the deformation of the solid skeleton, the effective per-

meability is so not constant. A well-known function converts initial intrinsic permeability k_0 into effective permeability based on effective porosity [25, 26]:

$$k = k_0 \left(\frac{\phi}{\phi_0} \right)^3 \left(\frac{1-\phi_0}{1-\phi} \right)^2. \tag{5}$$

The vapour transport includes two terms corresponding to Darcian advection and Fickian diffusion. It is reasonable to assume that the total pressure of gas mixture is almost constant and equals to the atmospheric pressure, so that the Darcian advection is negligible [21]. Thus, the velocity of vapour transport V_v only corresponds to Fickian diffusion which is written as follows:

$$V_v = -\frac{D\nabla\rho_v}{\rho_v} = -\frac{D_0 f \nabla\rho_v}{\rho_v} \tag{6}$$

where D, D_0, f represent the vapour diffusion coefficient, the free vapour diffusion coefficient in air, the resistance factor of pore network for gaseous diffusion respectively. f is a function of porosity ϕ and effective saturation S_w, which is given by:

$$f(S_w, \phi) = \phi(1-S_w)\phi^{x_D-1}(1-S_w)^{x_D+1} \tag{7}$$

where x_D is a material parameter. For granular media like soils, Millingon [27] suggested $x_D = 4/3$. In terms of cement and mortar, $x_D = 2.74$ is recommended [28]. $\phi(1-S_w)$ implies the actual space variable for vapour diffusion. $\phi^{x_D-1}(1-S_w)^{x_D+1}$ represents the tortuosity and connectivity effects.

The vapour is assumed as ideal gas in this research; thus the following relationship is obtained:

$$\rho_v = \frac{P_v M_v}{RT} \tag{8}$$

where P_v, M_v, R, T represent the vapour pressure, the vapour molar mass, the gas constant and the absolute temperature respectively.

The thermodynamic equilibrium between the liquid water and vapour is presumed. Thus, the Kelvin's equation shows the dependence of capillary pressure on relative humidity:

$$P_c = -\frac{\rho_w RT}{M_w} \ln \frac{P_v}{P_{vs}} \tag{9}$$

where P_{vs}, M_w represent the saturated vapour pressure and the water molar mass respectively.

Capillary pressure P_c is a discontinuity in pressure across the interface which is roughly equals to the difference between the gas mixture pressure P_g and the liquid water pressure P_w. Once the capillary pressure P_c is known, the saturation of liquid water S_w is immediately obtained by means of experimentally determined functions. The relationship of P_c is defined as a functional dependency on S_w, called the retention curve. For cement-based materials with low permeability, this curve is indirectly measured by sorption experiments implemented at constant temperature. Various models, including Brooks-Corey model and van Genuchten model, were proposed to describe the retention curve. In this paper, the well-accepted model proposed by van Genuchten is employed:

$$P_c(S_w) = \alpha\Big({S_w}^{-1/m} - 1\Big)^{1-m} \tag{10}$$

where α, m represent dimensionless parameters related to the pore-size distribution.

Relative permeability is an important variable which is also a functional dependency on S_w. Following the previous literatures [3, 25], a well-known and simple analytical relation derived from Genuchten-Mualem equation is chosen:

$$k_{rw} = {S_w}^{\ell}\left[1 - \Big(1 - {S_w}^{1/m}\Big)^{m}\right]^2. \tag{11}$$

where ℓ is a paramter which represents effects caused by tortuosity. The value $\ell = 0.5$ was proposed as the best choice for cement-based materials [29, 30].

Van Genuchten retention model also defines the moisture capacity $\partial S_w/\partial P_c$:

$$\frac{\partial S_w}{\partial P_c} = \frac{m}{\alpha(m-1)}{S_w}^{1/m}\Big(1 - {S_w}^{1/m}\Big)^{m}. \tag{12}$$

Substituting equations (4), (6) and (8-12) into mass balance equation (3) yields a standard governing equation for moisture transport in deformable porous medium:

$$-\phi\frac{\partial S_w}{\partial P_c}\cdot\frac{\partial P_w}{\partial t} + \nabla\cdot\left(-\frac{kk_{rw}}{\eta_w}\nabla P_w\right) - \frac{M_v P_{vs}}{RT\rho_w}\nabla\cdot\left[D_0 f\nabla e^{\left(\frac{M_w P_w}{\rho_w RT}\right)}\right] + S_w\frac{\partial\phi}{\partial t} = 0. \tag{13}$$

In the above equation, the second term represents the contribution of water advection and the third term indicates the contribution caused by vapour diffusion. The last term takes into account the impact of porosity variation for moisture transport. Combining a certain initial condition and

boundary conditions, the solution of moisture transport problem is accessible.

The moisture evaporation on the surface of porous media is mainly influenced by the interaction between porous media and the surrounding environment. The external moisture gradient, observed in the air in the vicinity of the open surface of porous media, governs the moisture transport from the interior of the porous media to its surface where evaporation happens. The Neumann-type boundary condition, which takes this given gradient into account, has been utilized in plenty of previous researches [3, 24, 31]. The formula is presented as follows:

$$w = \phi S_w^0 E \left(P_v^o - P_v^e\right), \tag{14}$$

where w represents the mass flux of moisture, P_v^0 the vapour pressure, P_v^e the surrounding vapour pressure and S_w^0 the water saturation within the media near the surface. The moisture exchange between the ambient environment and the porous media is mainly governed by emissivity E. A value $E = 2.58 \times 10^{-8} kg \cdot m^{-2} \cdot s^{-1} \cdot Pa^{-1}$ is measured for laboratory condition that there is no air flow and $T = 296 \pm 1K$ [32]. The term ϕS_w^0 represents the influence due to the decrease of wet surface when exposed to the environment with low RH.

It is necessary to notice that equation (10) is applied to main water vapour sorption isotherms. In this paper, we strictly focus on dynamic effects without discussing hysteresis. The dynamic effects are not exactly identical with hysteresis which is caused by ink-bottle effect, the variation of liquid-solid contact angle and the pore-size distribution and pore connectivity [11, 12]. Moreover, dynamic effects are dependent on change time rate of saturation and permeability [10, 13, 33]. Plenty of experiments proved that there exist dynamic effects when the saturation in porous medium surfers rapid fluctuation [8, 13, 34–37]. In fact, in the case of modelling with the rapid change of surrounding relative humidity, a dynamic model is indispensable to calculate a new $P_c - S_w$ relationship. The well-accepted equation (15), derived from thermodynamic theories and constitutive conservation laws, was mentioned firstly in [15]:

$$P_c^{dyn} - P_c = -\tau \frac{\partial S_w}{\partial t}. \tag{15}$$

The pressure difference between gas mixture and liquid water, indicated as P_c^{dyn}, is a measured

quantity during experiments. Meanwhile, the symbol P_c stands for equilibrium (or 'static') capillary pressure. The parameter τ is the dynamic effects coefficient, which serves as an assessment of the magnitude of dynamic capillarity effect. Since the gas mixture pressure could be assumed constant, the equation (15) reduces to the equation (16). The water pressure in the case of modeling with dynamic effects P_w^{dyn} should be used to replace the static water pressure P_w in moisture transport governing model:

$$P_w^{dyn} = P_w + \tau \frac{\partial S_w}{\partial t}. \tag{16}$$

Moreover, taking into account dynamic effects, Kelvin's equation (9) evolves into:

$$P_c^{dyn} = -\frac{\rho_w RT}{M_w} \ln \frac{P_v^{dyn}}{P_{vs}} \tag{17}$$

where P_v^{dyn} represents the dynamic vapour pressure. Practically, equations (16) and (17) govern the dynamic capillarity effect on water advection and vapour diffusion respectively. By submitting these relations to standard governing equation to replace the initially corresponding relations, it leads to the dynamic coupled model for vapour-water moisture transport:

$$\begin{aligned} -\phi \frac{\partial S_w}{\partial P_c} \cdot \frac{\partial P_w}{\partial t} + \nabla \cdot \left[-\frac{k k_{rw}}{\eta_w} \nabla \left(P_w + \tau \frac{\partial S_w}{\partial t} \right) \right] + S_w \frac{\partial \phi}{\partial t} \\ -\frac{M_v P_{vs}}{RT \rho_w} \nabla \cdot \left\{ D_0 f \nabla e^{\left[\frac{M_w}{\rho_w RT} \left(P_w + \tau \frac{\partial S_w}{\partial t} \right) \right]} \right\} = 0. \end{aligned} \tag{18}$$

The terms $\tau \frac{\partial S_w}{\partial t}$ in equation (18) represent the additional contribution on moisture transport induced by dynamic capillarity effect. The first one among them indicates the additional contribution caused by dynamic water advection. The second one stands for the additional contribution of dynamic vapour diffusion. Similar with the standard coupled model for moisture transport (equation 13), with certain given initial and boundary conditions, the dynamic moisture transport problem can be figured out.

2.2. Poro-mechanical model

The concept of effective stress $\sigma_{ij}^{'}$ is developed to model the behaviour of fully saturated porous media. It incorporates the impact of external load σ_{ij}, as well as the pore pressure P, into a single

term, defined as follows:

$$\sigma_{ij}^{'} = \sigma_{ij} - \zeta P \delta_{ij} \tag{19}$$

where δ_{ij} represents the Kronecker delta symbol. As given by [38], parameter $\zeta = 1 - K_b/K_s \leq 1$, where K_b is the drained bulk modulus of the porous material and K_s is the bulk modulus of its solid skeleton. Here, the positive values of stress and pore pressure denote compression.

The constitutive equations for an isotropic and fully saturated porous medium are written as follows:

$$\sigma_{ij} - (1 - K_b/K_s) P \delta_{ij} = 2\mu_b \varepsilon_{ij} + \lambda_b \varepsilon_v \delta_{ij} \tag{20}$$

where μ_b (shear modulus) and λ_b are known as Lame's moduli of dry media. ε_{ij} indicates strain tensor defined as $\varepsilon_{ij} = \left(\partial u_i/\partial x_j + \partial u_j/\partial x_i\right)/2$ and ε_v is a volumetric strain defined as $\varepsilon_v = \varepsilon_{xx} + \varepsilon_{yy} + \varepsilon_{zz}$.

Hence, only volumetric deformation could be caused by pore pressure. Therefore, in the absence of any external deviatoric stress loads and taking into account of the existing relation between bulk modulus and Lame's modulus i.e. $K_b = (2\mu_b + 3\lambda_b)/3$, the constitutive law (equation 20) reduces to:

$$\varepsilon_v = \frac{\overline{\sigma}}{K_b} - P\left(\frac{1}{K_b} - \frac{1}{K_s}\right) \tag{21}$$

where $\overline{\sigma}$ is volumetric stress, defined as the average of the trace of the stress tensor.

The constitutive law for unsaturated porous media can be achieved from the fully saturated system. In this paper, the discussion is limited to the case where all pores are occupied by two fluids which are water and air. As for unsaturated porous media, it is the acting averaged pressure surrounding the grains or solids [39]. Hence, replacing the initial pore pressure with an effective pore pressure obtained by using the averaging technique and assuming the immiscibility of the two phases, the constitutive law for unsaturated system is obtained:

$$\varepsilon_v = \frac{\overline{\sigma}}{K_b} - \left(S_w P_w + (1 - S_w) P_g\right)\left(\frac{1}{K_b} - \frac{1}{K_s}\right). \tag{22}$$

As for partially saturated porous media, capillary meniscus forms at the water-air interface and govern the pore pressure. Furthermore, the absolute value of water pressure rapidly exceeds the

atmospheric pressure during the drying process i.e. $\left|P_g\right| \ll |P_w|$. Thus, ignoring the contribution of the gas pressure and recalling the definition of capillary pressure $P_c = P_g - P_w$, the effective pore pressure reduces to $P = -S_w P_c$. Moreover, in the absence of any external loads, the poro-mechanical model (Eq. 22) reduces to the following equation:

$$\varepsilon_v = S_w P_c \left(\frac{1}{K_b} - \frac{1}{K_s}\right). \tag{23}$$

Coussy et al. [40] proposed an upgraded poro-mechanical model for cementitious materials by introducing the concept of equivalent pore pressure to substitute the effective pore pressure. This takes into account the additional contribution due to the release of interface energy during drying. Vlahinić [41] improved the initial model by providing the effective bulk modulus of the solid $\overline{K_s}$ to replace the initial constant K_s. It means that the bulk modulus of solid changes with drying is considered. In this work, we focus on dynamic capillarity effect, and strictly deal with the contribution of dynamic capillary pressure on skeleton deformation. For simplicity, the grains forming the matrix is assumed to be rigid, leading to $K_s \to \infty$. And the contribution of the interface energy is also neglected. So that, the initially simplest poro-mechanical model (Eq. 23) is employed to build the poro-mechanical model.

Submitting dynamic capillary pressure (Eq. 15) to substitute the corresponding standard capillary pressure in equation (23) and taking into account $1/K_s \approx 0$, the coupled dynamic model for predicting skeleton deformation is achieved:

$$\varepsilon_v = S_w \left(P_c - \tau \frac{\partial S_w}{\partial t}\right) \left(\frac{1}{K_b}\right) \tag{24}$$

Similarly, when the dynamic effects are taken into account, the constitutive equations for isotropic and partially saturated porous media are:

$$\sigma_{ij} - S_w \left(-P_c + \tau \frac{\partial S_w}{\partial t}\right) \delta_{ij} = 2\mu_b \varepsilon_{ij} + \lambda_b \varepsilon_v \delta_{ij} \tag{25}$$

The equilibrium equation which governs the solid deformation without neglecting body force ρb_i is given as follows:

$$\sigma_{ij,j} + \rho b_i = 0 \tag{26}$$

The combination of equations (18) and (26) leads to the fully coupled model which could take into account dynamic capillarity effect and governs the studied phenomenon. To obtain the numerical solution of basic variables water pressure P_w and displacement u, both initial and boundary conditions should be provided. The Neumann-type boundary condition is used for water pressure field and the external displacement or traction boundary conditions for displacement field (see Appendix).

3. Presentation of the numerical test

3.1. Modelling method

In order to obtain quantitative solutions for the proposed model, an appropriate numerical algorithm has been chosen. The governing equations are discretized in space by finite element method and in time by an implicit time-stepping method which is backward Euler method. The Galerkin method is used to get access to a weak form of the governing equations. The basic variables of the studied phenomenon are displacement u and water pressure P_w. They are expressed by global shape function matrices $\mathbf{N}^u$ and $\mathbf{N}^p$ as function of nodal value vectors $\mathbf{u}$ and $\mathbf{p_w}$: $\mathbf{U} = \mathbf{U}(t) = \mathbf{N}^u\mathbf{u}(t)$ and $P_w = P_w(t) = \mathbf{N}^p\mathbf{p_w}(t)$. According to the Galerkin method and Green's theorem, the following set of algebraic equations in space is obtained as follows by substituting these defined basic variables into governing equations (18) and (26) [42, 43]:

$$\mathbf{C_{ws}}\dot{\mathbf{u}} + \mathbf{P_{ww}}\dot{\mathbf{p}}_\mathbf{w} + \mathbf{H_{ww}}\mathbf{p_w} = \mathbf{f_w}, \tag{27}$$

$$\mathbf{Ku} - \mathbf{C_{dyn}}\dot{\mathbf{p}}_\mathbf{w} + \mathbf{C_{sw}}\mathbf{p_w} = \mathbf{f_u}. \tag{28}$$

The detailed derivation of the governing equations in discretised form is collected in Appendix. The meaning and full expression of the listed matrices can also be found in Appendix.

A two-dimensional plain strain hypothesis has been employed. The simulation is carried out using uniform mesh of 1750 rectangle elements for analysis. 50 elements on the length and 35 elements on the width. This mesh is sufficiently high to optimize the computing time and sufficiently small to well follow the fields. An implicit approximation (backward Euler method) in time step is

employed to guarantee the stability of the scheme. Furthermore, to solve the governing equations efficiently, the time step is adaptive according to the convergence rate.

As introduced previously, no existing literature considers a problem of moisture transport in a deforming porous media with dynamic effects accounted and very few documented experiment has been performed. One of these is a drying experiment for cement paste sample conducted by [44, 45], for which simulations performed with uncoupled standard model have been obtained by various researchers [3, 24]. This drying experiment has been used for the validation of the proposed coupled dynamic model.

To emphasize the influence of dynamic capillarity effect on moisture transport and skeleton deformation, three models including coupled standard model, uncoupled dynamic model and coupled dynamic model are employed to simulate the same drying experiment. Coupled standard model is used to simulate the moisture transport without considering the dynamic capillarity effect. By removing the terms relevant to dynamic effects in the coupled dynamic model, this model is easily achieved. As for an uncoupled dynamic model, it takes into account the dynamic capillarity effect, while totally neglects the performance of deformation. Thus, this model can also be obtained by eliminating the corresponding terms relevant to deformation in coupled dynamic model.

3.2. Experimental data

Experimental tests used for the comparison were performed by [44, 45]. Cement paste specimens were designed with Ordinary Portland Cement. Their properties are collected and summarised in Table 1. The cement pastes were cast in cylindrical mould with a diameter $d = 7cm$. Prior to

Table 1: Properties of cement paste I

Porosity	Initial RH	w/c	Young's modulus	Poisson's ratio	V-G Parameters	
					$\alpha(MPa)$	m
0.31	83%	0.35	29 (GPa)	0.26	44.75	0.48

drying experiment, the cement paste specimen has been cured for more than two hundred days in a sealed condition to reach physical (mechanism) and chemical stabilization. After removing the mould, the column was cut into $h = 10cm$ specimens. One end and the lateral surface of the sample were sealed with self-adhesive aluminium foil sheets. Only the other end was open for moisture

evaporation. As evaporation goes on, the induced pressure gradient in porous media transfers the inner moisture to open surface continuously (Figure 1). The drying experiments were performed

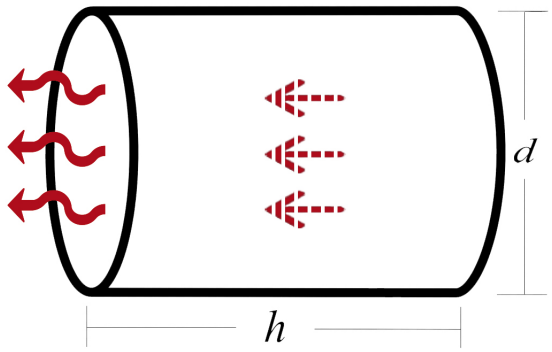

Figure 1: Schematic representation of drying

at a stable temperature T=296 $\pm$ 0.1K. The specimens were submitted to drying at two fixed external relative humidity 53.5% and 63.2% respectively. RH was fixed at $RH^e = 53.5\%$ by using a saturated salt solution (magnesium nitrate, $M_g(NO_3)_2 \cdot 6H_2O$). On the other hand, RH was fixed at $RH^e = 63.2\%$ by using solution of ammonium nitrate NH_4NO_3. Both of their mass loss curves were measured by weighing the specimens at intervals. No external load exists and the gravity is also neglected. Only axial deformation on the open end is allowed.

The main desorption isotherm curve is measured by the saturated salt solution method. The detailed description of the measurement is reported in [44]. The data related to main desorption isotherm were collected from literature [44, 45], and fitted according to the van Genuchten model to determine parameters a and m. The fitting curve is presented in Figure 2 and the corresponding parameter values are presented in Table 1. The values of mechanical properties are collected from previous literature [46] in which the mechanical properties of almost identical cement paste are measured. However, the important parameter permeability (or hydraulic conductivity) is unknown. In this paper, the inverse analysis method is adopted to fix the absent parameter.

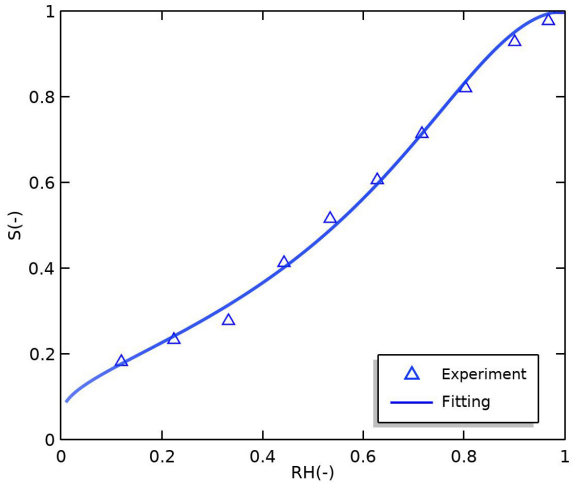

Figure 2: Van-Genuchten model fitting

4. Results analysis

4.1. Calculations with the coupled standard model

Firstly, the coupled standard model was used to simulate the drying experiment mentioned above. Intrinsic hydraulic conductivity K_w was determined independently by inversely analyzing the kinetics of mass loss during drying at a constant external relative humidity $RH^e = 53.5\%$ or $RH^e = 63.2\%$. The parameter optimization is based on the Levenberg-Marquardt (LM) algorithm. The mass loss is calculated by integrating the moisture mass evaporated from the open surface.

As presented in Figure 3, the fitting of hydraulic conductivity, which provides mass loss kinetics have high agreements with corresponding experimental data according to some conditions. Indeed, it must be noticed that the calibrated K_w values show dependency on boundary conditions. When the cement paste is exposed to environment with boundary condition $RH^e = 63.2\%$, $K_w = 2\times10^{-15}$ $m \cdot s^{-1}$ gives a good fitting of the mass loss with a correlation coefficient $R^2 = 0.980$ (Figure 3a), but it is not relevant for $RH^e = 53.5\%$. Inversely, when the boundary condition is $RH^e = 53.5\%$, $K_w = 3\times10^{-15}$ $m\cdot s^{-1}$ gives a good fitting of the mass loss with a correlation coefficient $R^2 = 0.988$ (Figure 3b), but it is not relevant for $RH^e = 63.2\%$. The relative deviation of these two calibrated results reaches to 33%. Moreover, the same drying experiment has also been simulated previously in literature [3]. Even though, the performance of deformation on moisture transport is ignored, a

difference in the permeability coefficient values is also recorded for cement pastes fitted by using two boundary conditions. It is consistent with the present calculations.

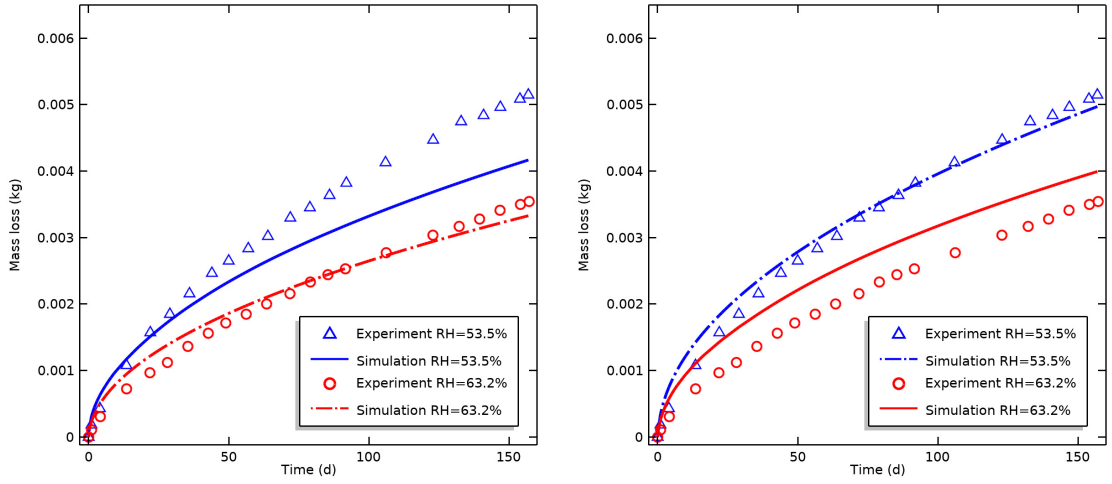

(a) Drying at $K_w = 2 \times 10^{-15} m \cdot s^{-1}$ (b) Drying at $K_w = 3 \times 10^{-15} m \cdot s^{-1}$

Figure 3: Comparisons of mass loss curves simulated by coupled standard model at identical permeability conditions with experimental results

Theoretically, K_w should be independent of the boundary condition; the previous researchers attribute such discrepancy to the variability of specimens preparation [3]. Nevertheless, we suppose that the observed discrepancy could be due to an added phenomenon, such as the dynamic capillarity effect.

4.2. Calculation with the coupled dynamic model

Drainage experiment in sand and soil proved that dynamic effects could accelerate the drainage, which inspires us to think about the same phenomenon may occur for drying in cement-based materials. Dynamic capillarity effect is positively relevant to the time change rate of water saturation $\partial S_w / \partial t$. Obviously, the lower external relative humidity 53.5%, causing a faster drying in porous media, leads to stronger dynamic effects. As the dynamic capillarity effect was ignored until now, the extra part of the mass loss supposed to be caused by dynamic effects can be supplemented by improving the transport coefficient, such as K_w. This is the main reason why the value of K_w fitted at lower drying condition $RH^e = 53.5\%$ is greater than that fitted at higher drying condition

$RH^e = 63.2\%$. The consideration of dynamic effects on capillary pressure is required for mass loss kinetics in porous media. In the coupled dynamic model, not only K_w but also dynamic effects coefficient τ plays an important role for calculation of drying process. Similarly to the coupled standard model, the unknown parameters are also determined by fitting mass loss kinetics of drying experiment.

As introduced previously, the investigation of dynamic effects coefficient is limited to quite permeable materials. Both of numerical analyses [47–49] and experimental methods [34, 50–53] were carried out to analyze this coefficient. As performed in [54], various numerical experiments for fine and coarse soil indicate τ ranges from 10^7 to $10^{10} kg \cdot m^{-1} s^{-1}$. The values of τ are recorded to range from 1.93×10^6 to $9.95 \times 10^9 kg \cdot m^{-1} s^{-1}$ in alternative references [52, 55]. Otherwise, plenty of studies concerning drainage experiments in sands for air-water systems [15] suggest that values of τ range from 3×10^4 to $5 \times 10^7 kg \cdot m^{-1} s^{-1}$. In total, τ in quite permeable materials, such as sand and soil, is likely in the range of 3×10^4 to $10^{10} kg \cdot m^{-1} s^{-1}$.

The results of coupled dynamic modelings with K_w values 2×10^{-15} and 3×10^{-15} $kg \cdot m^{-1} s^{-1}$ are presented and compared with the corresponding results of coupled standard modeling and experimental data in Figure 4 (a) and Fig. 4 (b) respectively. For these two K_w values, neither dynamic modeling nor standard modeling gives good fitting results for both boundary conditions. The dynamic and standard modeling results show slight deviation for high RH^e value and this deviation becomes significant as RH^e value is low. It implies that dynamic effects are stronger for fast drying.

Indeed, dynamic effects coefficient are dependent on intrinsic permeability, pore connectivity and effective saturation [10, 13, 33]. Several authors also have demonstrated the scale-dependence of dynamic effects [52, 56–58]. It is difficult to detect coherence between different investigations concerning the impacts of properties of fluids and porous materials on magnitude of τ and how it varies with saturation [16, 50, 54]. Stauffer [13] has presented an empirical formula to estimate τ for soil:

$$\tau = \frac{a \phi \eta_w}{kn} (H_{ce})^2 \tag{29}$$

where a is assumed to be constant and equal to 0.1 for quite permeable porous media. H_{ce} and

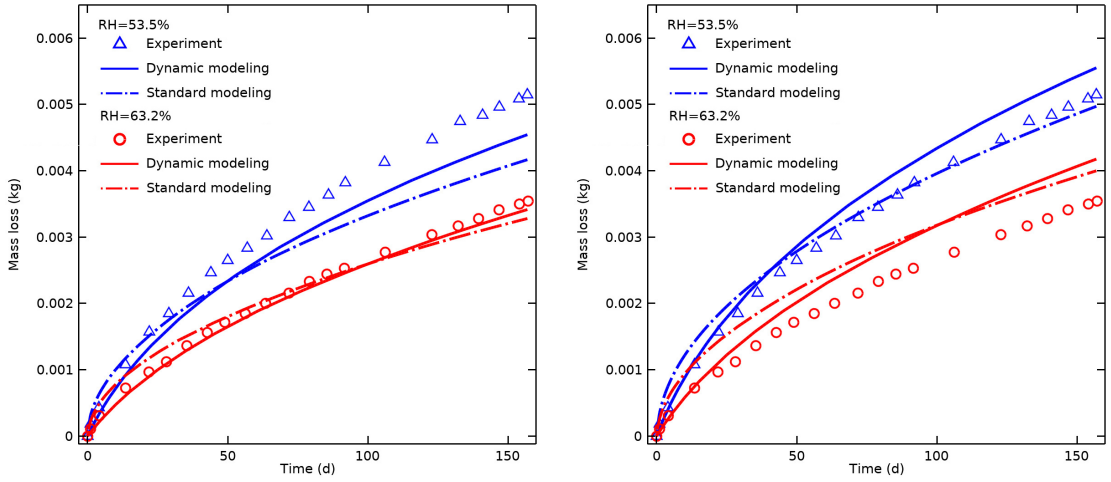

(a) Drying at $K_w = 2 \times 10^{-15} m \cdot s^{-1}$ (b) Drying at $K_w = 3 \times 10^{-15} m \cdot s^{-1}$

Figure 4: Comparisons of mass loss curves simulated by coupled dynamic and coupled standard modelings with experimental results

n represent coefficients in the Brooks-Corey formula. Although this empirical formula proved to be limited, we can at least effectively draw a conclusion that the dynamic effects coefficient is inversely proportional to the permeability. Thus, it is appropriate to suppose that the dynamic effects coefficient for weakly permeable porous media, such as cement-based materials, is greater than the largest one observed in soil.

Since the values of τ are difficult to determine, until now there is no well accepted formula to calculate its value. Recently, the drainage experiments [34] observed that $\tau - S_w$ almost follows log-linear function within a certain saturation range. They proposed a function given as $\log_{10}\tau = A(S_0 - S_w) + \log_{10}\tau_0$, in which S_0 and τ_0 are some threshold values and A is the slope of the lines, to fit the $\tau - S_w$ data. We note that we only did preliminary optimizations here. This log-linear function is employed to define the relation $\tau - S_w$. For coupled dynamic modeling, the unknown parameters are determined to provide the modeled mass loss curves equal to the measured data for both boundary conditions. The calibrated parameters are collected in table 2.

Table 2: Fitting results from inverse analysis of drying kinetics according to coupled dynamic model

$K_w(m \cdot s^{-1})$	$\tau_0(kg \cdot m^{-1}s^{-1})$	A	S_0	$R^2(RH^e = 53.5\%)$	$R^2(RH^e = 63.2\%)$
2.4×10^{-15}	8.91×10^{14}	3.74	0.83	0.992	0.988

In Figure 5 (a) the mass loss curves obtained from coupled dynamic modeling with adjusted K_w value $2.4 \times 10^{-15}\ kg \cdot m^{-1}s^{-1}$ are plotted and compared with the experimental measurements. Even though the same value K_w is used for both boundary conditions, all fitting results are quite good. The $R^2 = 0.992$ for boundary condition $RH^e = 53.5\%$ and $R^2 = 0.988$ for boundary condition $RH^e = 63.2\%$. However, as the same calibrated parameters are used for the case of coupled standard modeling, deviations become significant between modeling mass loss curves and experimental data especially for low ambient relative humidity condition $RH^e = 53.5\%$ (Figure 5 (b)). Nonetheless, there is no considerable variation between dynamic and non-dynamic modelings for high external relative humidity condition $RH^e = 63.2\%$ (red curves in Figure 5). Indeed, the higher external relative humidity induces slower drying. Considering dynamic effects are greatly dependent on drying rate, dynamic capillarity effect is weak for condition $RH^e = 63.2\%$. By comparing Figure 5 (a) and Figure 5 (b) and reviewing the poor performance of coupled standard model presented in Figure 3, the results computed by coupled standard model are not as good as that obtained from coupled dynamic model. Based on the verifications by the experimental data, it can be concluded that consideration of dynamic effects for moisture transport in cement-based materials is more advanced. The slight discrepancy observed between dynamic modeling curves and experimental data could be attributed to a potential reason that the relative permeability-saturation relationship is not independent and derived from the initial capillary pressure-saturation relationship. However, a constitutive relationship defined under steady-state conditions cannot be applied to transient flow procedures. Nonetheless, we strictly deal with the dynamic effects within the capillary pressure and ignore possible dynamic effects in the relative permeability curves. Another possible reason is that the prescribed log-linear function for $\tau - S_w$ relationship may slightly deviate from the reality. Considering the log-linear function has already given good fitting results and the available experimental data are limited, the improvement for $\tau - S_w$ relationship is arduous but fruitless. In addition, the order of magnitude of dynamic effects coefficient almost reaches to 1×10^{15} which is greater than the maximum one for soil. It is consistent with expectation discussed previously.

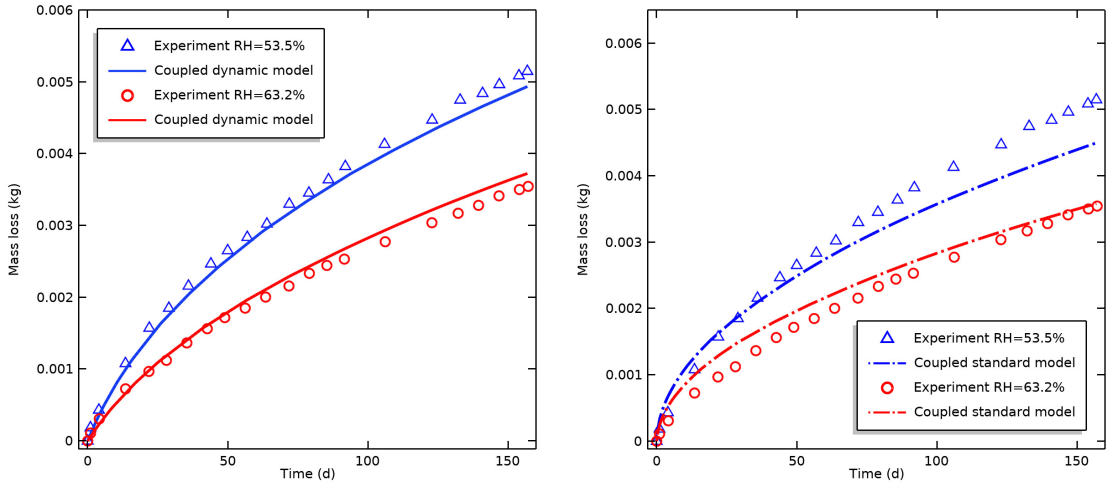

(a) Coupled dynamic modeling (b) Coupled standard modeling

Figure 5: Comparisons of modeling mass loss curves with experimental results.

5. Discussion

5.1. Spatiotemporal evolution of saturation

The spatiotemporal evolution of saturation for the studied cases obtained from coupled dynamic modeling is given by the maps in Figure 6. In this paper, we define the part of the material with a saturation disturbed by the variations of RH^e as the penetration depth. As presented in Figure 6, the penetration depth increases gradually as time goes by. the comparison of Figure 6 (a) with Figure 6 (b) shows that the differences in terms of penetration depth for both boundary conditions are not obvious. However, at the area close to open surface, the saturation obtained from modeling at condition $RH^e = 53.5\%$ is smaller than that obtained from modeling at condition $RH^e = 63.2\%$. The higher the hydric gradient between the external environment and the specimen, the faster the evaporation rate is. It indicates that the low external relative humidity accelerates the evaporation of vapour on open surface. Given the low saturation results in high capillary pressure, which enhances the generation and development of deformation.

The time change rate of saturation $\partial S_w/\partial t$ is calculated and plotted as a function of time and position in Figure 7. As expected, the absolute values of $\partial S_w/\partial t$ are extremely small for weakly permeable materials. The maximum absolute value is found at the position close to open surface

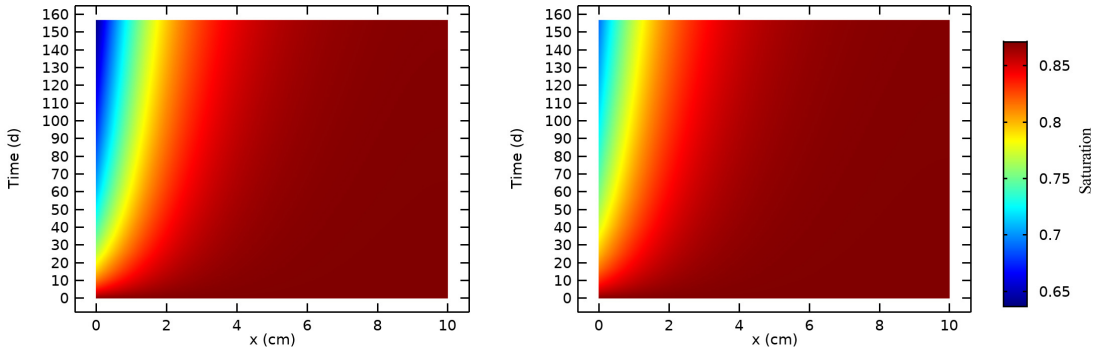

(a) Drying at $RH^e = 53.5\%$ (b) Drying at $RH^e = 63.2\%$

Figure 6: Spatiotemporal evolution of the saturation for both boundary conditions.

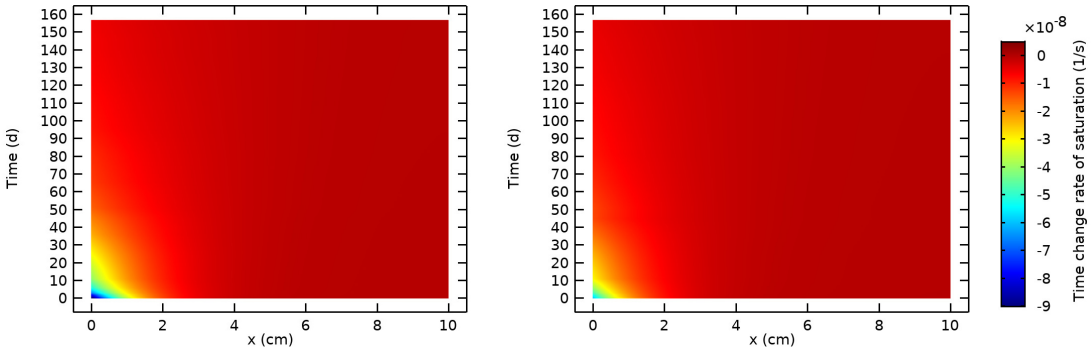

(a) Drying at $RH^e = 53.5\%$ (b) Drying at $RH^e = 63.2\%$

Figure 7: Spatiotemporal evolution of the time change rate of saturation for both boundary conditions.

during initial stage. As time goes by, the change rate decreases step by step. By comparing Fig. 7 (a) and Figure 7 (b), the change rate at condition $RH^e = 53.5\%$ is slightly faster than that at condition $RH^e = 63.2\%$. Indeed, the lower RH^e condition induces higher hydric gradient resulting in fast evaporation. By retrospecting the coupled dynamic model in previous section, the additional term describing the contribution of dynamic effects in dynamic model is greatly dependent on time change rate of saturation. Thus, the faster time change rate of saturation leads to stronger dynamic effects.

5.2. Fluid-solid coupling with the consideration of dynamic effects

After the verification of the dynamic coupled model, the performances of dynamic effects on coupling of moisture transport are discussed in this section. The investigations focus on the drying

procedure at condition $RH^e = 53.5\%$, since the low RH^e condition results in a relatively higher drying rate (Figure 7) and lower saturation state, inducing more significant dynamic capillarity effect and deformation. The investigation is implemented on the basis of results comparison regarding coupled dynamic modeling, uncoupled dynamic modeling and coupled standard modeling.

The result comparison between dynamic coupled modeling and dynamic uncoupled modeling aims to study the possible impact of deformation on moisture transport. The coupled dynamic model takes into account the effect of the skeleton deformation on moisture state evolution, while the uncoupled dynamic modeling totally neglects it. As presented in Figure 8, the mass loss curve of drying kinetics at $RH^e = 53.5\%$ obtained from uncoupled dynamic modeling are plotted and compared with that simulated by coupled dynamic model. Obviously, the mass loss curves of both simulations are almost identical. It indicates that the influence of deformation on moisture transport is limited. Indeed, the effective hydraulic conductivity is the main factor to determine moisture transport in porous media. One possible reason behind this phenomenon is that the contribution of deformation on the decrease of effective hydraulic conductivity is insignificant. In the dynamic modelling, after reach a certain time point, the mass loss has always higher values than the standard modelling. Considering capillary pressure is the driving force relevant to moisture transport, it confirms once again that dynamic effects on capillary pressure have non-negligible influence on drying process. Indeed, the observed phenomenon has clear theory foundation. As mentioned previously, the last three terms of coupled dynamic model (Eq. 18) have taken into consideration the contribution of dynamic effects on Darcian advection and Fickian diffusion. The fast drying induced by current boundary condition leads the dynamic effects can no longer be ignored.

Indeed, the proposed model can handle system experiencing significant deformation. Now, we propose to study fictitious experiments by using coupled dynamic model. In addition to giving an extremely low ambient relative humidity condition $RH^e = 10\%$ and providing additional two smaller Young's modulus values 3 and 5 GPa, the experimental setup and the cement paste and fluid properties almost remain unchanged. In this way, considerable deformation of cement paste occurs and then makes it possible to investigate the potential impact of deformation on drying procedure. We note that we only did preliminary qualitative analysis here. The mass loss curves of

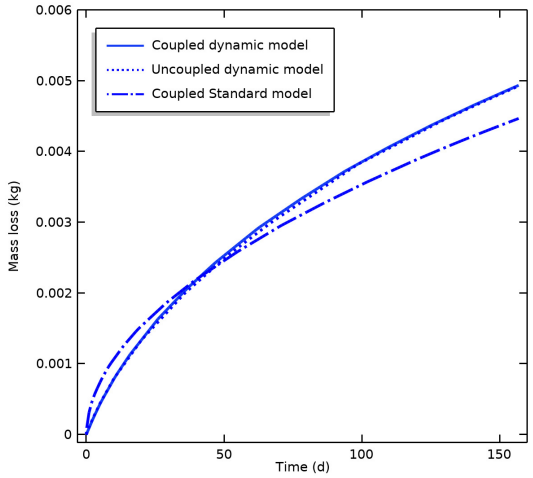

Figure 8: Comparisons of mass loss curves simulated by coupled dynamic modeling with results of uncoupled dynamic modeling and coupled standard modeling for $RH^e = 53.5\%$ condition.

the given system simulated by different values of Young's modulus are presented in Figure 9. The observed discrepancy between these three curves intuitively indicates that the deformation has an impact on moisture transport under extreme conditions.

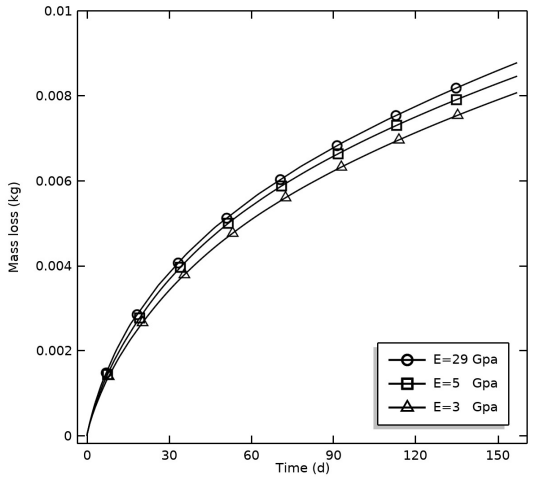

Figure 9: Modeling mass loss curves at condition $RH^e = 10\%$.

The numerical results of the axial displacement simulated by both dynamic and standard modelings are plotted and compared at various points of time during drying process in Figure 10.

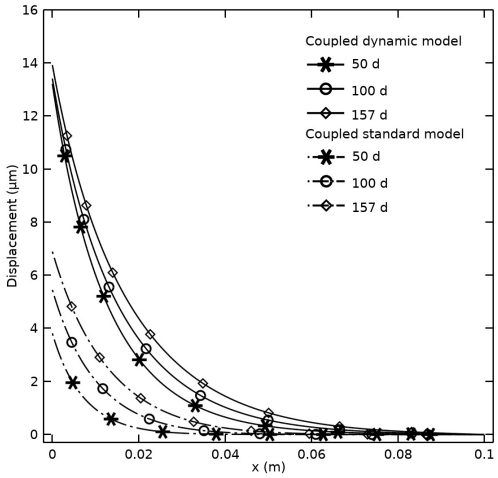

Figure 10: Comparison of axial displacement between dynamic and standard modeling.

Generally, both axial displacements increase gradually from sealed end to open surface. The slopes of these curves are increasing as position closes to open surface. However, axial displacement obtained from coupled dynamic modeling is always greater than that simulated by the standard coupled model along the axis. It indicates that dynamic effects could cause additional deformation for porous media during drying. Moreover, the position closer to the open surface, the greater deviation is observed between dynamic and standard modeling results. A rational explanation is given as follows. The dynamic term in constitutive model (equation 25) implies the contribution of dynamic effects on deformation generation. Theoretically, the strength of dynamic effects is proportional to time change rate of saturation and this rate is relatively high in the vicinity of the open surface of specimen during initial stage (Figure 7). Thus, it can be concluded that dynamic effects have a non-negligible impact on deformation under fast drying condition. Thereafter, the distributions of effective hydraulic conductivity simulated by both models are compared in Figure 11. Since the variation of hydraulic conductivity is relevant to deform according to equation (5), a phenomenon similar to the shrinkage evolution is founded. Although the maximum reduction of hydraulic conductivity is observed near open surface; this reduction is still relatively small.

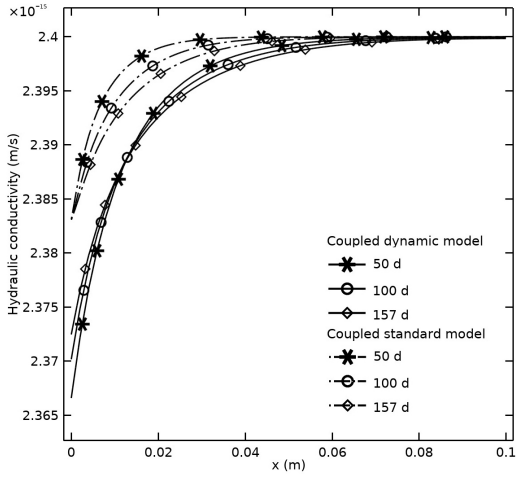

Figure 11: Comparison of effective hydraulic conductivity between dynamic and standard modeling.

6. Conclusions

In this study, a coupled dynamic model, which implements the dynamic capillarity effect and fluid-solid coupling into moisture transport, has been proposed and employed to simulate a drying experiment. The simulations in the case of coupled standard modeling (no dynamic effects) and uncoupled dynamic modeling (no fluid-solid coupling) have also been performed. Based on the verifications by the experimental data, the following conclusions can be drawn:

1) Compared with the traditional standard model, the dynamic model is more advanced and complete since the dynamic capillarity effect for the Darcian advection and Fickian diffusion has been considered. In addition, the investigation on the values of dynamic effects coefficient for cement-based materials is pioneering. The obtained values are greater than the values observed in soil, which are consistent with theoretical predictions.

2) Comparisons with measured mass loss curves for cement paste, drying experiments show that modeling taking dynamic effects into account obviously provides better results than the non-dynamic modeling. The main reason is that the dynamic model could predict the capillary pressure closer to actual value for moisture transport, especially in the condition that the vicinity of the open surface is exposed to variations of RH^e.

3) The mass loss curve of drying kinetics at $RH^e = 53.5\%$ obtained from coupled dynamic modeling, in which skeleton deformation is considered, has a good agreement like that obtained from uncoupled dynamic modeling, in which no deformation is allowed. It reveals that the influence of skeleton deformation on moisture transport is negligible for this kind of cement paste.

4) According to the comparisons performed in this paper, it is explicit that dynamic effects could cause additional unexpected displacement and increase the possibility of cracking risk, when the material strength is weak and/or the environmental conditions are extremes. Thus, dynamic capillarity effect should be taken into account for predicting durability of cement-based materials under low ambient relative humidity condition.

All conclusions are based on experimental and simulated results obtained on a kind of cement paste. More cement pastes and other weakly permeable porous material e.g. mortars and concretes should be employed to implement further verifications. Climate change conditions expected in the future (more wetting-drying cycles, more hot weather periods, etc.) should be simulated.

Appendix

In order to implement efficient numerical process, the governing equation for moisture transport (18) can be transformed to the following form:

$$-\phi\frac{\partial S_w}{\partial P_c}\cdot\frac{\partial P_w}{\partial t}+\nabla\cdot\left[\left(-\frac{kk_{rw}}{\eta_w}-\frac{M_wM_vD_0fP_v^{dyn}}{\left(RT\rho_w\right)^2}\right)\nabla\left(P_w+\tau\frac{\partial S_w}{\partial t}\right)\right]+S_w\frac{\partial\phi}{\partial t}=0. \qquad (30)$$

By introducing the finite element approximation $p_w = p_w(t) = \mathbf{N}^p\mathbf{p_w}(t)$ and using the Galerkin method, the weak form of moisture transport governing equation is obtained. After application of

the Green?s theorem and imposition of the boundary conditions, the weak form is given as below:

$$\begin{aligned}
&\int_{\Omega} \mathbf{N^{p,T}} \cdot \left(-\phi \frac{\partial S_w}{\partial P_c}\right) \mathbf{N^p} + \nabla \mathbf{N^{p,T}} \cdot \left(\frac{k k_{rw}}{\eta_w} + \frac{M_w M_v D_0 f P_v^{dyn}}{(RT\rho_w)^2}\right) \nabla \left(-\tau \frac{\partial S_w}{\partial P_c} \mathbf{N^p}\right) d\Omega \cdot \dot{\mathbf{p}}_{\mathbf{w}} \\
&+ \int_{\Omega} \nabla \mathbf{N^{p,T}} \cdot \left(\frac{k k_{rw}}{\eta_w} + \frac{M_w M_v D_0 f P_v^{dyn}}{(RT\rho_w)^2}\right) \cdot \nabla \mathbf{N^p} d\Omega \cdot \mathbf{p_w} \\
&+ \int_{\Omega} \mathbf{N^{p,T}} \cdot S_w \cdot \frac{\partial \phi}{\partial \varepsilon_v} \cdot \mathbf{m^T} \cdot \mathbf{B} d\Omega \dot{\mathbf{u}} \\
&+ \int_{\Gamma} \mathbf{N^{p,T}} \cdot \mathbf{q_\Gamma} d\Gamma = 0,
\end{aligned} \tag{31}$$

where $\mathbf{q_\Gamma} = \left(-\frac{k k_{rw}}{\eta_w} - \frac{M_w M_v D_0 f P_v^{dyn}}{(RT\rho_w)^2}\right) \cdot \nabla \left(P_w + \tau \frac{\partial S_w}{\partial t}\right) \cdot \mathbf{n}$ is the Neumann boundary conditions on Γ and $\mathbf{B} = \mathbf{L} \cdot \mathbf{N^u}$ with $\mathbf{L}$ the differential operator. In addition, $\mathbf{m}$ is a vector equivalent to Kronecker δ_{ij}. Thus, the algebraic equation of moisture transport (27) in space is obtained as the following definitions are employed:

$$\mathbf{C_{ws}} = \int_{\Omega} \mathbf{N^{p,T}} \cdot S_w \cdot \frac{\partial \phi}{\partial \varepsilon_v} \cdot \mathbf{m^T} \cdot \mathbf{B} \cdot d\Omega, \tag{32}$$

$$\mathbf{P_{ww}} = \int_{\Omega} \mathbf{N^{p,T}} \cdot \left(-\phi \frac{\partial S_w}{\partial P_c}\right) \mathbf{N^p} + \nabla \mathbf{N^{p,T}} \cdot \left(\frac{k k_{rw}}{\eta_w} + \frac{M_w M_v D_0 f P_v^{dyn}}{(RT\rho_w)^2}\right) \nabla \left(-\tau \frac{\partial S_w}{\partial P_c} \mathbf{N^p}\right) d\Omega, \tag{33}$$

$$\mathbf{H_{ww}} = \int_{\Omega} \nabla \mathbf{N^{p,T}} \cdot \left(\frac{k k_{rw}}{\eta_w} + \frac{M_w M_v D_0 f P_v^{dyn}}{(RT\rho_w)^2}\right) \cdot \nabla \mathbf{N^p} d\Omega, \tag{34}$$

$$\mathbf{f_w} = -\int_{\Gamma} \mathbf{N^{p,T}} \cdot \mathbf{q_\Gamma} d\Gamma, \tag{35}$$

On the basis of the principle of virtual work and Green's theorem, the weak form of the equilibrium equation (26) is given as follows:

$$-\int_{\Omega} \partial \varepsilon^{\mathbf{T}} \cdot \sigma_{ij} \cdot d\Omega + \int_{\Gamma_t} \partial \mathbf{U^T} \cdot \mathbf{t} \cdot d\Gamma + \int_{\Omega} \partial \mathbf{U^T} \cdot \rho \cdot \mathbf{b} \cdot d\Omega = 0, \tag{36}$$

where $\partial\mathbf{U}$ is arbitrary infinitesimal displacement. $\partial\varepsilon = \mathbf{L}\cdot\partial\mathbf{U}$ is the infinitesimal strain corresponding to $\partial\mathbf{U}$. Γ_t is natural boundary, i.e. the boundary condition is imposed as traction for displacement field: $\mathbf{t} = \sigma_{ij}\mathbf{n}$. Here, the outward unit normal vector to the boundary surface is denoted by $\mathbf{n}$. Moreover, after substitution of effective stress principle and the constitutive relationship into equation (36) and elimination of the common arbitrary factor the algebraic form of the governing equation for skeleton deformation (28) is obtained if the following definitions are employed:

$$\mathbf{C_{sw}} = \int_{\Omega} \mathbf{B^T}\cdot\zeta\cdot S_w\cdot\mathbf{m}\cdot\mathbf{N^P}\cdot d\Omega, \tag{37}$$

$$\mathbf{C_{dyn}} = \int_{\Omega} \mathbf{B^T}\cdot\zeta\cdot S_w\cdot\tau\frac{\partial S_w}{\partial p_c}\cdot\mathbf{m}\cdot\mathbf{N^P}\cdot d\Omega, \tag{38}$$

$$\mathbf{f_u} = \int_{\Omega} \mathbf{N^{u,T}}\cdot\rho\cdot\mathbf{b}\cdot d\Omega + \int_{\Gamma_t} \mathbf{N^{u,T}}\cdot\mathbf{t}\cdot d\Gamma, \tag{39}$$

$$\mathbf{Ku} = \int_{\Omega} \mathbf{B^T}\sigma' d\Omega = \int_{\Omega} \mathbf{B^T D B} d\Omega\mathbf{u}, \tag{40}$$

where $\mathbf{D}$ is the constitutive matrix of the material and $\mathbf{K}$ the global stiffness matrix. Finally, the full discretisation in time by considering the Euler implicit scheme allows the algebraic equations (27) and (28) reach to equations (41) and (42) respectively:

$$\mathbf{C_{ws}^{n+1}}\frac{\mathbf{u}^{n+1}-\mathbf{u}^n}{\delta t_n} + \mathbf{P_{ww}^{n+1}}\frac{\mathbf{p_w}^{n+1}-\mathbf{p_w}^n}{\delta t_n} + \mathbf{H_{ww}^{n+1}}\mathbf{p_w}^{n+1} = \mathbf{f_w}^{n+1}, \tag{41}$$

$$\mathbf{Ku}^{n+1} - \mathbf{C_{dyn}^{n+1}}\frac{\mathbf{p_w}^{n+1}-\mathbf{p_w}^n}{\delta t_n} + \mathbf{C_{sw}^{n+1}}\mathbf{p_w}^{n+1} = \mathbf{f_u}^{n+1}, \tag{42}$$

where superscript $n{+}1$ indicates that the nonlinear system is written at time $t_{n+1} = t_n{+}\delta t_n$ with δt_n the time increment. For given initial conditions $\mathbf{u}^0$ and $\mathbf{p_w^0}$, the solution of the nonlinear system $(\mathbf{p_w}^{n+1}, \mathbf{u}^{n+1})$ is computed for all $n = 0, \cdots, N-1$. This system is solved by Newton-Raphson algorithm.

Acknowledgments

Authors would like to thank the China Scholarship Council for the financial support (PhD grant). Also the National Centre for Scientific Research (CNRS) is acknowledged for the financial support of the project DUMP (DEFI INFINITI 2017).

References

[1] E. Holt, M. Leivo, Cracking risks associated with early age shrinkage, Cement and Concrete Composites 26 (2004) 521–530.

[2] J. Carette, F. Benboudjema, G. Nahas, K. Abahri, A. Darquennes, R. Bennacer, Concrete drying: effects of boundary conditions and specimen shape, Service Life of Cement-Based Materials and Structures (2016) 385.

[3] Z. Zhang, M. Thiery, V. Baroghel-Bouny, Numerical modelling of moisture transfers with hysteresis within cementitious materials: Verification and investigation of the effects of repeated wetting–drying boundary conditions, Cement and Concrete Research 68 (2015) 10–23.

[4] R. Day, J. Illston, The effect of rate of drying on the drying/wetting behaviour of hardened cement paste, Cement and Concrete Research 13 (1983) 7–17.

[5] S. M. Hassanizadeh, Advanced theories of two-phase flow in porous media, Handbook of porous media (2015) 47–62.

[6] P. S. Huyakorn, Computational methods in subsurface flow, academic press, 2012.

[7] G. Topp, A. Klute, D. Peters, Comparison of water content-pressure head data obtained by equilibrium, steady-state, and unsteady-state methods 1, Soil Science Society of America Journal 31 (1967) 312–314.

[8] D. Smiles, G. Vachaud, M. Vauclin, A test of the uniqueness of the soil moisture characteristic during transient, nonhysteretic flow of water in a rigid soil 1, Soil Science Society of America Journal 35 (1971) 534–539.

[9] H. W. Brown, Capillary pressure investigations, Journal of Petroleum Technology 3 (1951) 67–74.

[10] S. M. Hassanizadeh, M. A. Celia, H. K. Dahle, Dynamic effect in the capillary pressure–saturation relationship and its impacts on unsaturated flow, Vadose Zone Journal 1 (2002) 38–57.

[11] K. K. Aligizaki, Pore structure of cement-based materials: testing, interpretation and requirements, CRC Press, 2014.

[12] R. M. Espinosa, L. Franke, Inkbottle pore-method: prediction of hygroscopic water content in hardened cement paste at variable climatic conditions, Cement and Concrete Research 36 (2006) 1954–1968.

[13] F. Stauffer, Time dependence of the relations between capillary pressure, water content and conductivity during drainage of porous media, in: IAHR symposium on scale effects in porous media, Thessaloniki, Greece, volume 29, 1978, pp. 3–35.

[14] S. M. Hassanizadeh, W. G. Gray, Mechanics and thermodynamics of multiphase flow in porous media including interphase boundaries, Advances in Water Resources 13 (1990) 169–186.

[15] S. M. Hassanizadeh, W. G. Gray, Thermodynamic basis of capillary pressure in porous media, Water Resources Research 29 (1993) 3389–3405.

[16] G. Barenblatt, T. W. Patzek, D. Silin, The mathematical model of nonequilibrium effects in water-oil displacement, SPE journal 8 (2003) 409–416.

[17] R. Helmig, A. Weiss, B. I. Wohlmuth, Dynamic capillary effects in heterogeneous porous media, Computational Geosciences 11 (2007) 261–274.

[18] X. Cao, I. Pop, Degenerate two-phase porous media flow model with dynamic capillarity, Journal of Differential Equations 260 (2016) 2418–2456.

[19] C.-Z. Qin, B. Guo, M. Celia, R. Wu, Dynamic pore-network modeling of air-water flow through thin porous layers, Chemical Engineering Science (2019).

[20] F. Wittmann, On the action of capillary pressure in fresh concrete, Cement and Concrete Research 6 (1976) 49–56.

[21] M. Mainguy, O. Coussy, V. Baroghel-Bouny, Role of air pressure in drying of weakly permeable materials, Journal of Engineering Mechanics 127 (2001) 582–592.

[22] O. Coussy, Mechanics and physics of porous solids, John Wiley & Sons, 2011.

[23] Z. Zhang, M. Thiéry, V. Baroghel-Bouny, Analysis of moisture transport in cementitious materials and modelling of drying-wetting cycles, in: International Conference: Numerical Modeling Strategies for Sustainable Concrete Structures, The French Association of Civil Engineering (AFGC), Aix-en-Provence, France, 2012.

[24] Z. Zhang, M. Thiery, V. Baroghel-Bouny, Investigation of moisture transport properties of cementitious materials, Cement and Concrete Research 89 (2016) 257–268.

[25] V. Genuchten, M. Th, A closed-form equation for predicting the hydraulic conductivity of unsaturated soils 1, Soil Science Society of America Journal 44 (1980) 892–898.

[26] B. Bary, A. Sellier, Coupled moisture—carbon dioxide–calcium transfer model for carbonation of concrete, Cement and Concrete Research 34 (2004) 1859–1872.

[27] R. Millington, Gas diffusion in porous media, Science 130 (1959) 100–102.

[28] M. Thiery, V. Baroghel-Bouny, N. Bourneton, G. Villain, C. Stéfani, Modélisation du séchage des bétons: analyse des différents modes de transfert hydrique, Revue européenne de génie civil 11 (2007) 541–577.

[29] H. Ranaivomanana, J. Verdier, A. Sellier, X. Bourbon, Prediction of relative permeabilities and water vapor diffusion reduction factor for cement-based materials, Cement and Concrete Research 48 (2013) 53–63.

[30] S. Zamani, R. Kowalczyk, P. McDonald, The relative humidity dependence of the permeability of cement paste measured using garfield nmr profiling, Cement and Concrete Research 57 (2014) 88–94.

[31] S. Dal Pont, F. Meftah, B. Schrefler, Modeling concrete under severe conditions as a multiphase material, Nuclear engineering design 241 (2011) 562–572.

[32] M. Azenha, K. Maekawa, T. Ishida, R. Faria, Drying induced moisture losses from mortar to the environment. part ii: numerical implementation, Materials and Structures 40 (2007) 813–825.

[33] G. Goel, L. K. Abidoye, B. R. Chahar, D. B. Das, Scale dependency of dynamic relative permeability–satuartion curves in relation with fluid viscosity and dynamic capillary pressure effect, Environmental Fluid Mechanics 16 (2016) 945–963.

[34] L. Zhuang, S. M. Hassanizadeh, C. Z. Qin, A. de Waal, Experimental investigation of hysteretic dynamic capillarity effect in unsaturated flow, Water Resources Research 53 (2017) 9078–9088.

[35] A. Elzeftawy, R. Mansell, Hydraulic conductivity calculations for unsaturated steady-state and transient-state flow in sand 1, Soil Science Society of America Journal 39 (1975) 599–603.

[36] G. Vachaud, M. Vauclin, M. Wakil, A study of the uniqueness of the soil moisture characteristic during desorption by vertical drainage 1, Soil Science Society of America Journal 36 (1972) 531–532.

[37] D. Wildenschild, J. Hopmans, J. Simunek, Flow rate dependence of soil hydraulic characteristics, Soil Science Society of America Journal 65 (2001) 35–48.

[38] M. Biot, D. Willis, The elastic coefficients of the theory of consolidation, J. appl. Mech 24 (1957) 594–601.

[39] B. A. Schrefler, The finite element method in the deformation and consolidation of porous media, Wiley, 1987.

[40] O. Coussy, P. Dangla, T. Lassabatère, V. Baroghel-Bouny, The equivalent pore pressure and the swelling and shrinkage of cement-based materials, Materials and Structures 37 (2004) 15–20.

[41] I. Vlahinić, H. M. Jennings, J. J. Thomas, A constitutive model for drying of a partially saturated porous material, Mechanics of Materials 41 (2009) 319–328.

[42] B. A. Schrefler, R. Scotta, A fully coupled dynamic model for two-phase fluid flow in deformable porous media, Computer methods in applied mechanics and engineering 190 (2001) 3223–3246.

[43] B. A. Schrefler, Z. Xiaoyong, A fully coupled model for water flow and airflow in deformable porous media, Water Resources Research 29 (1993) 155–167.

[44] V. Baroghel-Bouny, Water vapour sorption experiments on hardened cementitious materials: Part i: Essential tool for analysis of hygral behaviour and its relation to pore structure, Cement and Concrete Research 37 (2007) 414–437.

[45] M. D. Nguyen, Modélisation des couplages entre hydratation et dessiccation des matériaux cimentaires à l'issue du décoffrage, thesis, 2009.

[46] C.-J. Haecker, E. Garboczi, J. Bullard, R. Bohn, Z. Sun, S. Shah, T. Voigt, Modeling the linear elastic properties of portland cement paste, Cement and Concrete Research 35 (2005) 1948–1960.

[47] E. Diamantopoulos, W. Durner, Dynamic nonequilibrium of water flow in porous media: A review, Vadose Zone Journal 11 (2012).

[48] V. Joekar-Niasar, S. Hassanizadeh, Specific interfacial area: The missing state variable in two-phase flow equations?, Water Resources Research 47 (2011).

[49] H. K. Dahle, M. A. Celia, S. M. Hassanizadeh, Bundle-of-tubes model for calculating dynamic effects in the capillary-pressure-saturation relationship, Transport in Porous Media 58 (2005) 5–22.

[50] T. Sakaki, D. M. O'Carroll, T. H. Illangasekare, Direct quantification of dynamic effects in capillary pressure for drainage–wetting cycles, Vadose Zone Journal 9 (2010) 424–437.

[51] W. Lo, C. Yang, S. Hsu, C. Chen, C. Yeh, M. Hilpert, The dynamic response of the water retention curve in unsaturated soils during drainage to acoustic excitations, Water Resources Research 53 (2017) 712–725.

[52] D. B. Das, M. Mirzaei, Dynamic effects in capillary pressure relationships for two-phase flow in porous media: Experiments and numerical analyses, AIChE Journal 58 (2012) 3891–3903.

[53] G. Camps-Roach, D. M. O'Carroll, T. A. Newson, T. Sakaki, T. H. Illangasekare, Experimental investigation of dynamic effects in capillary pressure: Grain size dependency and upscaling, Water Resources Research 46 (2010).

[54] M. Peszynska, S.-Y. Yi, Numerical methods for unsaturated flow with dynamic capillary pressure in heterogeneous porous media, Numer. Anal. Model 5 (2008) 126–149.

[55] M. Mirzaei, D. B. Das, Dynamic effects in capillary pressure–saturations relationships for two-phase flow in 3d porous media: Implications of micro-heterogeneities, Chemical Engineering Science 62 (2007) 1927–1947.

[56] S. Bottero, S. M. Hassanizadeh, P. Kleingeld, T. Heimovaara, Nonequilibrium capillarity effects in two-phase flow through porous media at different scales, Water Resources Research 47 (2011).

[57] G. Goel, D. M. O'Carroll, Experimental investigation of nonequilibrium capillarity effects: Fluid viscosity effects, Water Resources Research 47 (2011).

[58] L. K. Abidoye, D. B. Das, Scale dependent dynamic capillary pressure effect for two-phase flow in porous media, Advances in Water Resources 74 (2014) 212–230.

Contribution of the capillary pressure second-order term on fast drying of cement-based materials

Yuliang Zou[a,b], Frédéric Grondin[a,*], Mazen Saad[b],

[a]Institut de Recherche en Génie Civil et Mécanique (GeM), CNRS UMR 6183, Centrale Nantes, 1 rue de la Noë, 44321 Nantes, France

[b]Laboratoire de Mathématiques Jean Leray (LMJL), CNRS UMR 6629, Centrale Nantes, 1 rue de la Noë 44321 Nantes, France

yuliang.zou@ec-nantes.fr

frederic.grondin@ec-nantes.fr (corresponding author)

mazen.saad@ec-nantes.fr